Cirrus cloud simulations using WRF with improved radiation parameterization and increased vertical resolution

Y. Gu,[1] K. N. Liou,[1] S. C. Ou,[1] and R. Fovell[1]

Received 2 June 2010; revised 7 January 2011; accepted 14 January 2011; published 30 March 2011.

[1] The capability of Weather Research and Forecasting (WRF) model in the simulation of cirrus clouds has been examined, with a focus on the effects of radiative processes and vertical model resolution. We incorporate in WRF a new radiation module, referred to as the Fu-Liou-Gu scheme, which is an improvement and refinement based on the Fu-Liou scheme, particularly in reference to parameterization of the single-scattering properties of ice crystal size and shape. We conducted a number of real-time WRF simulations for cirrus cases that were observed in the coastal and western United States on 29–30 March 2007, and we compared these with available observations from Moderate Resolution Imaging Spectroradiometer (MODIS) and GOES visible and IR images over the same areas. Simulation results show that WRF is capable of generating reasonable cirrus cloud fields and their movement and dissipation processes, especially those associated with the large-scale frontal system. Radiative processes are important in cirrus cloud simulations by affecting the vertical thermal structure and hence convection. The newly implemented radiation module, the Fu-Liou-Gu scheme, has been demonstrated to work well in WRF and can be effectively used for studies related to cirrus cloud formation and evolution and aerosol-cloud-radiation interactions. With the newly implemented radiation scheme, the simulations of cloud cover and cloud and ice water path (CWP and IWP) have been improved for cirrus clouds, with a more consistent comparison with the corresponding MODIS observations in terms of CWP and IWP means and CWP frequency distribution, especially for optically thin cirrus with an improvement of about 20% in simulated mean IWP. The model-simulated ice crystal sizes have also been shown to be comparable to those determined from MODIS cloud products. Finally, we have demonstrated that model vertical resolution plays a significant role in cirrus cloud simulation in terms of altering vertical velocity field and the associated regional circulation.

Citation: Gu, Y., K. N. Liou, S. C. Ou, and R. Fovell (2011), Cirrus cloud simulations using WRF with improved radiation parameterization and increased vertical resolution, *J. Geophys. Res.*, *116*, D06119, doi:10.1029/2010JD014574.

1. Introduction

[2] Cirrus clouds cover about 20% of the Earth's surface and play an important role in the radiation field of the Earth-atmosphere system and significantly affect the atmospheric thermal structure and climate [*Liou*, 1986, 1992]. Cirrus clouds are a dynamic and thermodynamic system that involves the intricate coupling of microphysics, radiation, and dynamic processes [*Gultepe and Starr*, 1995]. A multidimensional setting is thus required for interaction and feedback studies. A number of modeling studies have been performed to investigate cirrus cloud formation processes [e.g., *Starr and Cox*, 1985; *Heymsfield and Sabin*, 1989; *Sassen and Dodd*, 1989; *Jensen et al.*, 1994a, 1994b; *DeMott et al.*, 1994]. In their pioneering work, *Starr and Cox* [1985] developed a two-dimensional (2-D) model and showed that the effects of radiative processes and vertical transports are both significant in cirrus cloud formation and maintenance. *Gu and Liou* [2000] constructed a 2-D cirrus model to investigate the interaction and feedback of radiation, ice microphysics, and turbulence-scale turbulence and their influence on the evolution of cirrus clouds, and reported that radiation and its interaction with microphysical and dynamical processes play an important role in the formation and evolution of these clouds. The 2-D cloud-resolving models with smaller scales are ideal for microscopic process simulations involving the evolution of a cirrus cloud with explicit ice microphysics. However, other influences on cirrus cloud formation and evolution may occur on the synoptic or mesoscale, such as a large tropical convective cloud system that generates extensive cirrus anvils and newly generated

[1]Joint Institute for Regional Earth System Science and Engineering, Department of Atmospheric and Oceanic Sciences, University of California, Los Angeles, California, USA.

0148-0227/11/2010JD014574

cirrus. These kinds of systems cannot readily be examined using a 2-D cloud-resolving model. Also, a 2-D cloud-resolving model can become numerically unstable after a few hours of simulations due to its very small spatial scales and is not suitable for simulations of cirrus clouds associated with large-scale systems that can last for days.

[3] While numerical models have been extensively used to study cirrus clouds, it is critically important to examine how reliable the models are in terms of reproducing cirrus cloud fields. For instance, one of the modeling uncertainties is the simulation of thin cirrus clouds which are important to atmospheric radiation budget [*Forster et al.*, 2007]. Also, comparisons of the ice water content (IWC) measurements from the Earth Observing System's Microwave Limb Sounder (MLS) with those simulated from global climate models show substantial disagreements, which occur over eastern Pacific, Atlantic Intertropical Convergence Zones, tropical Africa, and South America [*Li et al.*, 2005]. Improvements of model physics (e.g., radiation parameterization) and model dynamics (e.g., increasing horizontal and vertical resolution) are big issues in terms of the generation of realistic representations of cirrus cloud distribution. Among them, the parameterization of cloud/radiation processes in global and regional climate models is a complex task. Radiative transfer in the atmosphere is determined by spectrally dependent optical properties of atmospheric gases and clouds. Calculation of the radiative heating/cooling in clouds is complicated due to difficulties in parameterizing their single-scattering properties, especially those of ice clouds due to complexities in the ice crystal size, shape, and orientation which cannot be determined from the models [*Liou*, 1986].

[4] Model development (on model dynamics) has been confined mostly to increasing horizontal resolution; however, the vertical resolution has been usually kept at certain levels, for example, about 20 levels for GCMs [*Ruti et al.*, 2006]. Using a single-column model, *Tompkins and Emanuel* [2000] have demonstrated that the vertical distribution of water vapor in GCMs can be very sensitive to model vertical resolution. Additionally, the effects of increasing vertical resolution on climate simulation in terms of more realistic cloud spectrum and water vapor have been presented by *Inness et al.* [2001], *Pope et al.* [2001], and *Spencer and Slingo* [2003]. *Starr and Wylie* [1990] reported that the vertical resolution in mesoscale cirrus cloud process models should be of the order of 50 m to adequately capture the true character of the cloud generation and maintenance processes.

[5] The Weather Research and Forecasting (WRF) model, a high-resolution regional model, can be used to perform real-case cirrus cloud simulations. However, its performance in terms of realistic representation of the cirrus cloud distribution in the atmosphere requires examination and in-depth investigation. Also, the existing radiation schemes in WRF treat the cloud effect, which is the most important regulator of the radiation field in the Earth-atmosphere system, in a rather crude manner. The objective of this paper is to implement a new radiation module with improved parameterizations for ice crystal effective size and single-scattering properties in the WRF for studies related to cirrus clouds, to assess the WRF's capability to simulate cirrus clouds by comparison with satellite observations, and to investigate the effects of radiation parameterization and vertical resolution on model simulations.

[6] The paper is organized as follows: Section 2 synthesizes model characteristics and new module for radiation parameterization. Section 3 describes the experiment design, real case simulations, and comparison with satellite observations. Section 3 also presents a discussion on experiment results regarding the effects of radiation and vertical resolution in cirrus simulations. Conclusions are given in section 4.

2. Implementation of a New Radiation Module in WRF

[7] The WRF model version 2.2 [*Skamarock et al.*, 2005] is a fully compressible, nonhydrostatic model (with a hydrostatic option) suitable for a broad spectrum of applications across scales ranging from a few meters to thousands of kilometers. Currently, several physics components have been included in WRF: microphysics (bulk schemes ranging from simplified physics suitable for mesoscale modeling to sophisticated mixed-phase physics suitable for cloud-resolving modeling), cumulus parameterization, longwave radiation, shortwave radiation, boundary layer turbulence, surface layer, land-surface parameterization, and subgrid-scale diffusion.

[8] For radiative transfer associated with clouds, the current schemes in WRF normally use preset tables to represent shortwave and longwave processes associated with clouds. For shortwave radiation, the current choices in WRF include the Dudhia scheme [*Dudhia*, 1989] with a simple downward integration of solar flux, accounting for clear-air scattering, water vapor absorption, and cloud albedo and absorption which use look-up tables; the ETA GFDL shortwave scheme in which the doubling/adding method [*Lacis and Hansen*, 1974] is used for solar radiation, but absorption due to other gases such as O_2 is not accounted for; or the Goddard shortwave scheme, which employs a modified delta-Eddington approximation. Also included is the NCAR CAM radiation scheme, in which the delta-Eddington approximation is employed for solar radiative transfer coupled with an absorptivity-emissivity formulation for IR radiation transfer. The longwave radiation schemes employed in the present WRF model either use preset tables [*Mlawer et al.*, 1997] to represent longwave processes due to water vapor, ozone, carbon dioxide, and trace gases (if present) as well as accounting for cloud optical depth (RRTM scheme) or follow the simplified exchange method of *Fels and Schwarzkopf* [1975] and *Schwarzkopf and Fels* [1991] with calculation over spectral bands associated with carbon dioxide, water vapor, and ozone (ETA GFDL longwave scheme). Recently, a new version of RRTM-RRTMG, which includes the Monte Carlo independent column approximation (MCICA) method for random cloud overlap, has been incorporated in the WRF model.

[9] To improve the computation of radiative transfer processes in the current WRF model, a more physically based, consistent, and efficient radiation scheme that can better resolve the spectral bands, determine the cloud optical properties, and provide more reliable and accurate radiative heating fields is needed. The new radiation module, the Fu-Liou-Gu scheme [*Gu et al.*, 2010], that we implement in WRF is a modified and improved version based on the Fu-Liou radiative transfer model [*Fu and Liou*, 1992, 1993], which provides new and better parameterizations for ice

crystal effective size and single-scattering properties to accommodate a specific treatment of mixed ice crystal shapes to represent more realistic ice radiative effects based on observations, and to broaden radiation parameterization by including a variety of aerosol types. The detailed description of the model and the relevant parameters used in this scheme have been given by *Fu and Liou* [1992, 1993]. A combination of the delta-four-stream approximation for solar flux calculations [*Liou et al.*, 1988] and delta-two-and-four-stream approximation for IR flux calculations [*Fu et al.*, 1997] has been implemented in this scheme. This combination has been proven to be computationally efficient and at the same time to produce a high degree of accuracy. The incorporation of nongray gaseous absorption in multiple scattering atmospheres is based on the correlated *k*-distribution method developed by *Fu and Liou* [1992]. The solar and IR spectra are divided into 6 and 12 bands, respectively, according to the location of absorption bands. In the solar spectrum, absorption due to H_2O (2500–14500 cm^{-1}), O_3 (50000–14500 cm^{-1}), CO_2 (2850–5200 cm^{-1}), and O_2 (A, B, and γ bands) is taken into account. In the thermal IR region, absorption due to H_2O (0–2200 cm^{-1}), CO_2 (540–800 cm^{-1}), O_3 (980–1100 cm^{-1}), CH_4 (1100–1400 cm^{-1}), N_2O (1100–1400 cm^{-1}), and CFCs (in the 10 μm region) is included. The continuum absorption of H_2O is accounted for in the spectral region 280–1250 cm^{-1}. In addition to the principal absorbing gases listed above [*Fu and Liou*, 1993; *Gu et al.*, 2003], we recently included absorption by the water vapor continuum and a number of minor absorbers in the solar spectrum, including CH_4, N_2O, NO_2, O_3, CO, SO_2, O_2-O_2, and N_2-O_2. This led to an additional absorption of solar flux in a clear atmosphere of the order of 1–3 W/m^2 depending on the solar zenith angle and the amount of water vapor employed in the calculations [*Zhang et al.*, 2005].

[10] The single-scattering properties for ice particles, including the extinction coefficient (β_e), the single-scattering albedo (ϖ), and the asymmetry factor (g), which are dependent on wavelength and the vertical position in the cloud, are parameterized in terms of ice water content (*IWC*) and mean effective size (D_e) in the forms [*Liou et al.*, 2008]

$$\beta_e(\lambda;x,y,z) = \mathrm{IWC}(x,y,z)\sum_{n=0}^{N}\left[a_n(\lambda)/D_e^n(x,y,z)\right], \quad (1)$$

$$\varpi(\lambda;x,y,z) = 1 - \sum_{n=0}^{N} b_n(\lambda)D_e^n(x,y,z), \quad (2)$$

$$g(\lambda;x,y,z) = \sum_{n=0}^{N} c_n(\lambda)D_e^n(x,y,z), \quad (3)$$

where a_n, b_n, and c_n are coefficients determined from numerical fitting based on detailed light-scattering and absorption calculations for a range of ice crystal size distributions and shapes based on scattering and absorption database provided by *Yang et al.* [2000] for the solar spectrum and *Yang et al.* [2005] for the thermal IR spectrum. For solar bands, the first-order polynomial expansion is sufficient to achieve 0.1% accuracy. However, for thermal IR bands, the second-order polynomial fitting is required to achieve this level of accuracy.

[11] More recently, we have also incorporated an ice microphysics parameterization to include an interactive mean effective ice crystal size (D_e) in connection with radiation parameterizations [*Liou et al.*, 2008]. Correlation analysis between IWC and D_e has been carried out using a large set of observed ice crystal size distributions obtained from a number of cirrus field campaigns in the tropics, midlatitude, and Arctic. It is showed that IWC and D_e are well correlated using this regional division. We used the χ^2 best fit to these observed data and obtained the best parameterization equation in polynomial as follows:

$$\ln(De) = \mathrm{a} + \mathrm{b}\ln(IWC) + \mathrm{c}(\ln(IWC))^2, \quad (4)$$

where the coefficients *a*, *b*, and *c* are listed in Table 1 for tropics, midlatitudes (warm and cold cirrus clouds, respectively), and Arctic. Ice crystal habit information for different regions is based on available observations and the mixture of ice crystal shapes varies with region in the parameterization [*Liou et al.*, 2008]. For the current study, parameterization of D_e for midlatitudes is employed, in which IWC ranges from ~10^{-4}–10^{-1} g/m^3, while D_e has values from ~30 to ~140 μm. Ice crystal shape consists of 60% bullet rosettes and aggregates, 20% hollow columns, and 20% plates for ice crystal maximum dimension (L) > 70 μm, while for L < 70 μm, the shape factor consists of 50% bullet rosettes, 25% plates, and 25% hollow columns [*Baum et al.*, 2000; *Liou et al.*, 2008]. Uncertainty in the measurement of small ice crystals <100 μm from aircraft platforms has been an important issue in scientific discussions. Shattering of millimeter-sized ice particles in collision with the probe can artificially enhance the concentration of small ice crystals [e.g., *Heymsfield et al.*, 2006]. Because of the uncertainty in small ice crystal measurements, we have conducted three independent *IWC*-D_e correlation experiments: (1) maximizing small ice crystals, (2) reducing concentration of these smaller ice crystals (N_{sm}) by 1 order of magnitude, and (3) reducing N_{sm} by 2 orders of magnitude. Experiment 2 was used as the base run, while the other two give a possible range of the parameterized D_e due to uncertainties in small ice crystal measurements. Uncertainty in small ice crystal measurements in the correlation leads to deviations from the mean by less than 2 W/m^2 in radiative forcing values, revealing that the base run D_e is an excellent parameter for radiation calculations [*Liou et al.*, 2008]. Having included all the preceding ice crystal size and shape features, the Fu-Liou-Gu scheme is now the most comprehensive scheme for the simulation of radiative transfer associated with cirrus clouds in weather and climate models.

[12] In the current Fu-Liou-Gu radiation scheme, a total of 18 aerosol types have been parameterized by employing the Optical Properties of Aerosols and Clouds (OPAC) database [*d'Almeida et al.*, 1991; *Tegen and Lacis*, 1996; *Hess et al.*, 1998], which provides the single-scattering properties for spherical aerosols computed from the Lorenz-Mie theory in which humidity effects are accounted for. The single-scattering properties of the 18 aerosol types for 60 wavelengths in the spectral region between 0.3 μm and 40 μm are interpolated into the 18 Fu-Liou spectral bands of the current radiation scheme [*Gu et al.*, 2006, 2010]. Aerosol types include maritime, continental, urban, five different sizes of mineral dust, insoluble, water soluble, soot

Table 1. Coefficients a, b, and c for D_e-IWC Correlations in Equation (2) for Tropics, Midlatitudes, and Arctic [*Liou et al.*, 2008]

		Midlatitude		
Coefficients	Tropics	Warm (−40° to −20°C)	Cold (−65° to −40°C)	Arctic
A	5.4199	5.2375	4.3275	4.8510
B	0.35211	0.13142	0.26535	0.33159
C	0.012680	0	0.021864	0.026189

(BC), sea salt in two modes (accumulation mode and coarse mode), mineral dust in four different modes (nucleation mode, accumulation mode, coarse mode, and transported mode), and sulfate droplets. The present radiation scheme therefore can also be used to study direct and indirect aerosol radiative effects in addition to cirrus clouds.

3. Real Case Cirrus Cloud Simulation and Validation

3.1. Case Description

[13] Cirrus cloud cover has been increasing over the northeastern Pacific Ocean since the 1970s, particularly during spring, due, in part, to increases in upper tropospheric and lower stratospheric humidity as well as the presence of increasing formation and spreading of contrails and contrail cirrus clouds as a result of trans-Pacific air traffic [*Minnis et al.*, 2004]. Over this same region, thin cirrus clouds were observed and reported by military pilots during test flights on 29 and 30 March 2007. For these reasons, we acquired relevant Moderate Resolution Imaging Spectroradiometer (MODIS)/Terra-Aqua daytime and nighttime images for 29 and 30 March 2007, over the northeastern Pacific Ocean and western United States. MODIS is a 36-channel spectroradiometric sensor that was installed on board both Terra and Aqua satellite platforms, which were launched in December 1999 and May 2001, respectively. Both Terra and Aqua are in Sun-synchronous polar orbits with daytime equator crossings at 1030 and 1330 LTC, respectively. Aqua is the leading platform of the A-Train constellation, which also include Cloud-Aerosol Lidar and Infrared Pathfinder Satellite Observations (CALIPSO) and CloudSat. MODIS has a 1 km^2 field of view mapping to a swath of approximately 2330 km with global data archived every day. MODIS data is divided into "granules. " Each granule is composed of 2030 lines of data, and each line is composed of 1350 pixels. The MODIS cloud product contains both physical and radiative cloud properties, including cloud mask, cloud-particle phase (ice versus water, clouds versus snow) mask, cloud top temperature/pressure/height, effective cloud-particle radius, and cloud optical depth. For comparison with WRF simulation results, MODIS granules over the eastern Pacific Ocean and western United States have been examined and scenes containing widespread cirrus clouds matching the WRF domain and simulation time period have been selected.

[14] The following is a list of MODIS images: Terra daytime on 29 March 2007 at 1825 UTC, Aqua daytime on 29 March 2007 at 2140 UTC, Terra nighttime on 30 March 2007 at 0530 UTC, and Aqua daytime on 30 March 2007 at 2045 UTC (as shown in Figures 1a–1d). For comparison purposes, we also acquired GOES 11 visible and IR images over the same general area from the NOAA Web site for the dates and times that were close to MODIS/Terra/Aqua overpasses: 29 March 2007 at 1830 UTC, 29 March 2007 at 2130 UTC, 30 March 2007 at 0530 UTC, and 30 March 2007 at 2030 UTC (as shown in Figures 1e–1h). Both MODIS and GOES 11 observations showed the presence of cirrus clouds in streaking and patchy patterns over coastal and western U.S. areas at the dates and times listed above. We have selected these cases for the WRF simulations to demonstrate its capability in generating cirrus cloud patterns that can match satellite cloud images.

3.2. Experiment Design

[15] On the basis of the observed cases, the model domain has been selected to center at 35°N–120 °W and cover the area from 135°−105° W and 20°–45° N. The horizontal resolution is 30 km and the bottom-top, south-north, and west-east dimensions are 28 × 97 × 112. Initial and boundary condition data used are the National Centers for Environmental Prediction (NCEP) Final (FNL) Operational Global Analysis on a 1.0 × 1.0 degree grid, continuously at every 6 h. This product is available from the Global Forecast System (GFS) that is operational four times a day in near real time at NCEP. We have performed 48 h model integrations in conjunction with the observed cases starting on 29 March 2007 at 0000 UTC. The accuracy of the initial condition plays an important role in the model simulations. However, it has been a common practice to employ one set of initial condition for model simulations of a real case using WRF for performance evaluation [e.g., *Li et al.*, 2008; *Zhang et al.*, 2010]. We have carried out additional case studies using initial conditions at different times and found insignificant differences between model results from different initializations.

[16] In accordance with our research objective, i.e., to examine the ability of WRF for the simulation of cirrus clouds and to investigate the effects of radiation processes and the vertical model resolution in the simulation, we have designed the following three experiments (see also Table 2).

[17] 1. The CTRL experiment is the control run in which the Lin ice microphysics scheme was used along with RRTM for longwave radiation and a solar radiation scheme based on a look-up table approach for cloud albedo and cloud absorption [*Dudhia*, 1989]. RRTM also uses preset tables [*Mlawer et al.*, 1997] to represent longwave radiative processes primarily associated with water vapor, ozone, carbon dioxide, and cloud optical depth. A vertical resolution with 28 model levels was used in this simulation.

[18] 2. The RADI experiment is identical to CTRL, except that the Fu-Liou-Gu radiation scheme was followed. Major improvements of the Fu-Liou-Gu scheme over the Dudhia and RRTM schemes include the treatment of clouds in terms of providing parameterizations based on theory and observations for ice crystal effective size and shape, and the associated spectral optical and single-scattering properties. This scheme also includes a parameterization for the spectral radiative properties of a variety of aerosol types, essential to investigate the direct and indirect radiative forcings of aerosol particles and their interactions with clouds.

[19] 3. In the VERT experiment, the number of model level in the RADI setup was increased from 28 to 65. Levels

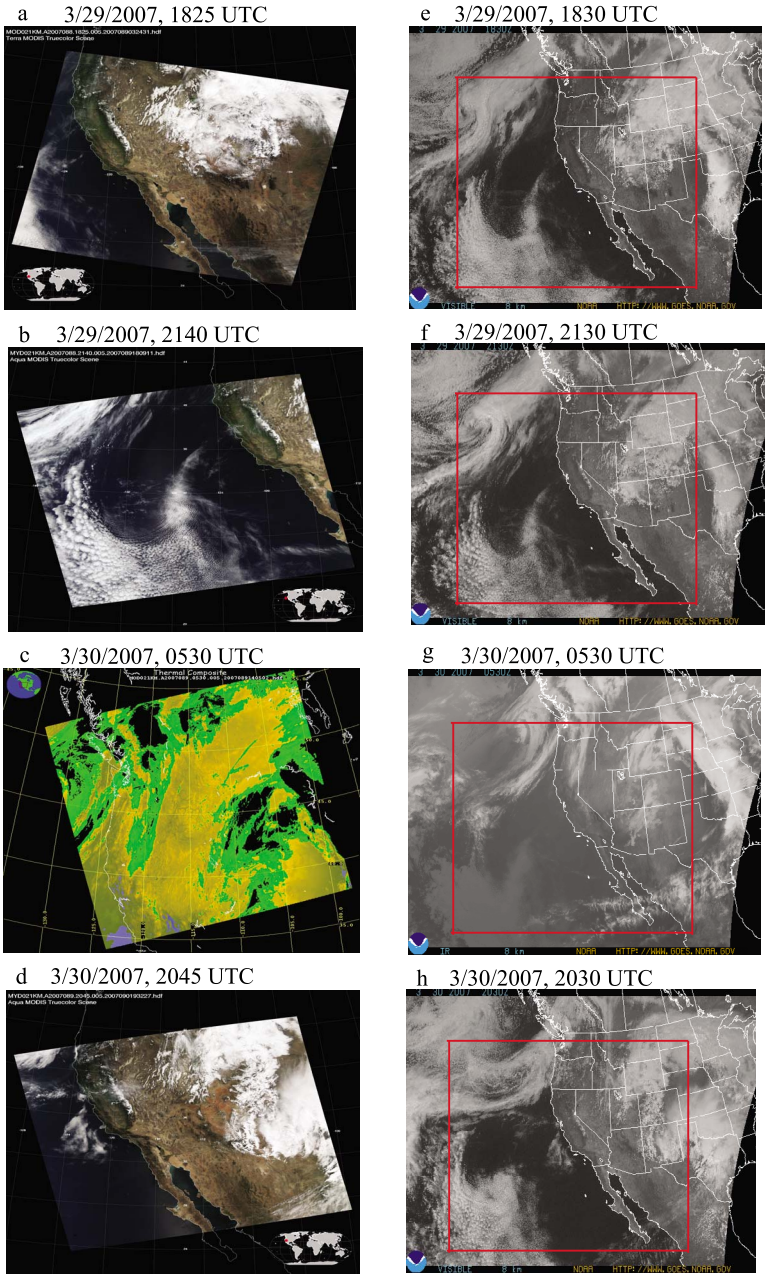

Figure 1. (a–d) Observed Moderate Resolution Imaging Spectroradiometer (MODIS) images at 1825 and 2140 UTC on 29 March and 0530 and 2045 UTC on 30 March 2007 and (e–h) GOES 11 visible and IR images at 1830 and 2130 UTC on 29 March and 0530 and 2030 UTC on 30 March 2007. The frame in the GOES 11 images represents the model domain.

above 500 mbar were added in order to capture the frequent occurrence of cirrus clouds at these levels, corresponding to an enhancement of averaged vertical resolution from about 1 km to less than 0.25 km.

3.3. Simulation of Cirrus Clouds and Comparison With Satellite Observations

[20] We first evaluate model performance by examining simulation results obtained from the preceding three experiments. Figures 2a–2d show the contour of simulated ice water path (IWP) from CTRL at 1800 UTC (Figure 2a) and 2200 UTC (Figure 2b) on 29 March; and 0600 UTC (Figure 2c) and 2100 UTC (Figure 2d) on 30 March 2007. Figures 2e–2h and Figures 2i–2l illustrate the simulation results determined from RADI and VERT, respectively. These results are compared with the corresponding MODIS

Table 2. Experiment Design

Experiment	Radiation Scheme	Vertical Levels
CTRL	solar, Dudhia scheme; infrared, RRTM scheme	28
RADI	Fu-Liou-Gu scheme	28
VERT	Fu-Liou-Gu scheme	65

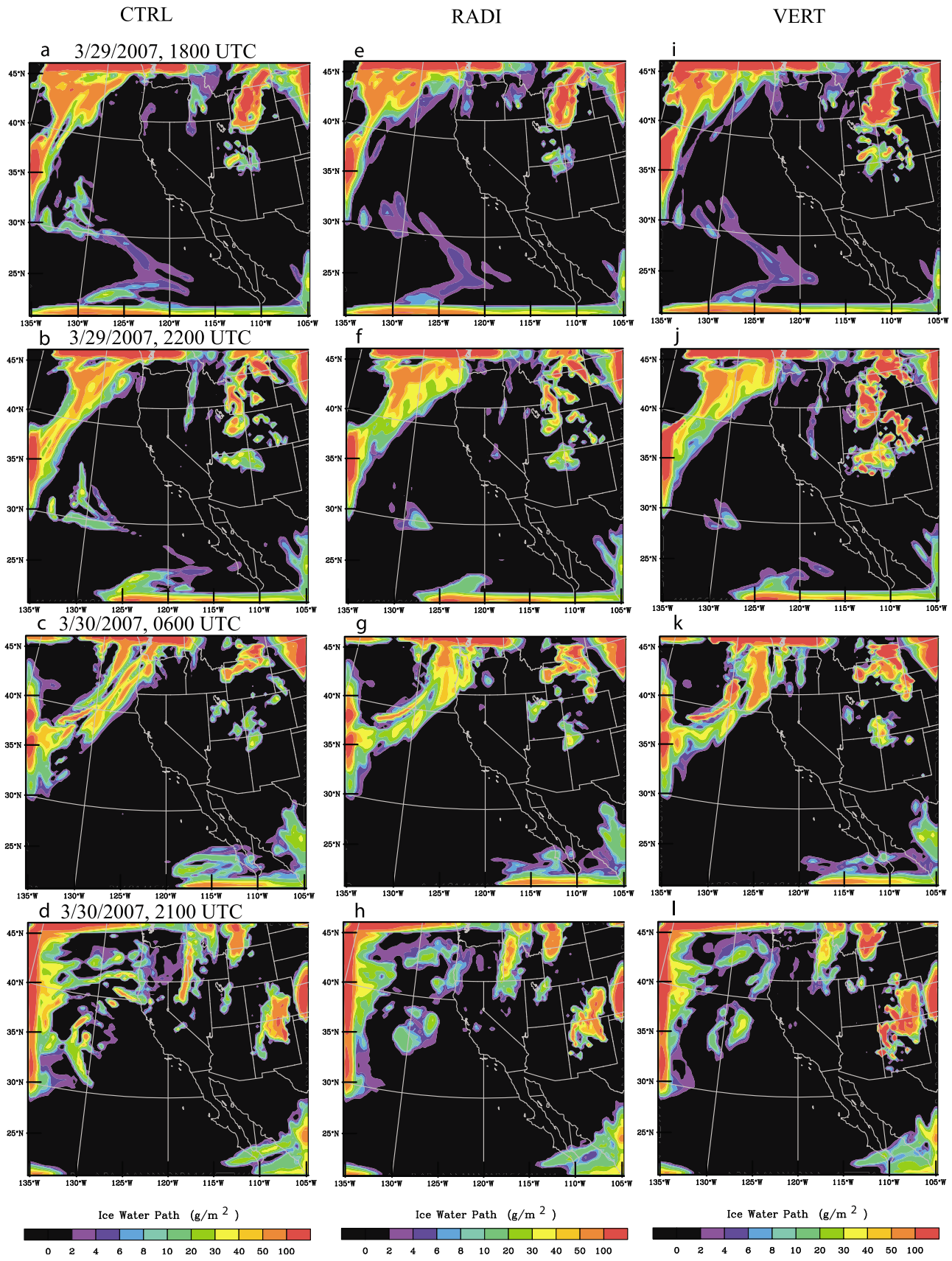

Figure 2. Model-simulated ice water paths (IWPs) from the experiments (a–d) CTRL, (e–h) RADI, and (i–l) VERT at 1800 and 2200 UTC on 29 March and at 0600 and 2100 UTC on 30 March 2007.

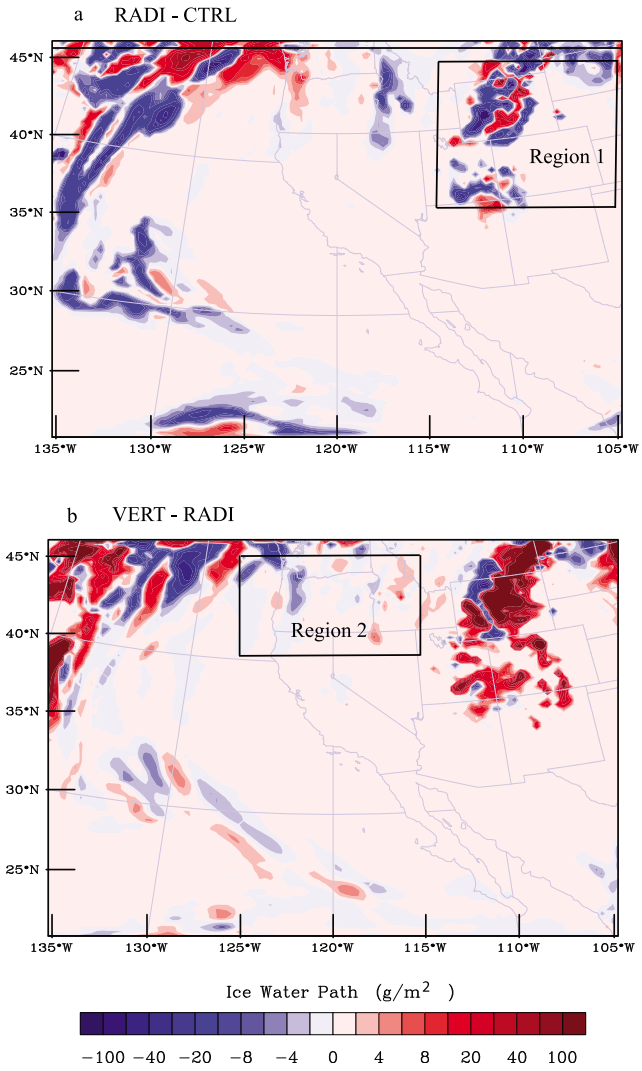

Figure 3. Simulated differences in IWP between (a) RADI and CTRL and (b) VERT and RADI at 1800 UTC, 29 March 2007. The boxes in Figure 3 show the two selected domains: 35°–45°N and 105°–115°W, covering Wyoming, Utah, and Colorado (Region 1, Figure 3a), and 40°–45°N and 115°–125°W, covering Oregon (Region 2, Figure 3b). The line near 45°N in Figure 3a indicates the cross section (*xz* plane) used in results for Figure 7.

(Figures 1a–1d) and GOES 11 (Figures 1e–1h) images, which display cirrus cloud cover close to the preceding times. The frame in the GOES 11 images represents the model domain. The three model simulations display the observed cirrus cloud patterns, including the clouds associated with the frontal system off the west coast and some nonfrontal ice clouds to the west of southern California and Mexico. Cirrus clouds over the western United States, including Wyoming, Utah, Colorado, Arizona, and New Mexico, as shown in both MODIS and GOES 11 images, have also been well simulated in the model. These clouds were not associated with the frontal system since they showed as patchy patterns on satellite images as well as modeling results. They did not move when the frontal system moved eastward during the 2 day period. On the basis of the work of *Wallace and Hobbs* [1977], as the warm front approaches, cirrostratus thickens and lowers and turns into altostratus. They appear patchy during this transition. MODIS cloud top temperature map shows that a significant number of pixels display warm temperatures around 240–250 K. Therefore it is possible that the clouds over Wyoming, Utah, and Colorado were undergoing transition from cirrostratus to altostratus and were nearly stationary. The frontal cirrus clouds off the west coast travel from west to east and move over land starting at 0600 UTC, 30 March 2007 (Figure 1g). This migration has been well reproduced from the model (Figures 2c, 2g, and 2k). The cloud dissipation process when clouds move over land has been demonstrated in both satellite observations and model simulations (Figure 1g and Figures 2c, 2g, and 2k).

[21] The effects of radiation and the vertical resolution on cirrus simulations can be examined by comparisons among the three experiments. Simulated differences in IWP between RADI and CTRL at 1800 UTC on 29 March 2007 (Figure 3a) demonstrate the effect of different radiation schemes used in the model, while those between VERT and RADI (Figure 3b) reveal the impact of increased vertical resolution on cloud cover.

[22] With the new radiation scheme, more cirrus clouds have been simulated near the cyclone center off the west coast and over central Oregon, as well as in the cloud center area over Wyoming (Figure 3a), with fewer clouds in the surrounding area. The corresponding downward solar flux at the surface displays negative (positive) changes when the cloud field has been enhanced (reduced) owing to the scattering and absorption of solar radiation by cloud particles (Figure 4a). The surface downward longwave radiation, on the other hand, increases (decreases) accordingly since the enhanced cloud field traps more IR fluxes, which are emitted back to the Earth (Figure 4c). To compare with the model-simulated ice cloud water, we have extracted the total cloud water path (CWP) available from the MODIS L-2 cloud product database for the two domains: 35°–45°N and 105°–115°W, covering Wyoming, Utah, and Colorado (Region 1, see Figure 3a) and 40°–45°N and 115°–125°W, covering Oregon (Region 2, see Figure 3b) at 1825 UTC on 29 March 2007. The latter region involves semitransparent thin cirrus clouds. MODIS data sets contain information of the optical depth and a mean effective particle size for high-level ice clouds. This information is used to derive CWP on the basis of the formulation CWP = $4\rho\tau r_e/3Q_e$, where ρ is the water density, τ is the cloud optical depth, and r_e is the cloud particle radius [*Stephens*, 1978]. MODIS data sets do not contain IWP, which is a product of IWC and cloud thickness. To obtain a reasonable IWP for comparison with model-simulated values, we have followed a parameterization approach developed by *Liou et al.* [2008] in which the cloud optical depth, IWP, and the mean effective radius for cirrus clouds are related by

$$\tau = IWP\left(e_0 + e_1/a_e + e_2/a_e^2\right), \tag{5}$$

where IWP is the ice water path in gm/m^2, a_e is half of the mean effective ice crystal size, and e_0, e_1, and e_2 are the fitting coefficients, which were determined from thousands of ice crystal size distributions collected by airborne in situ

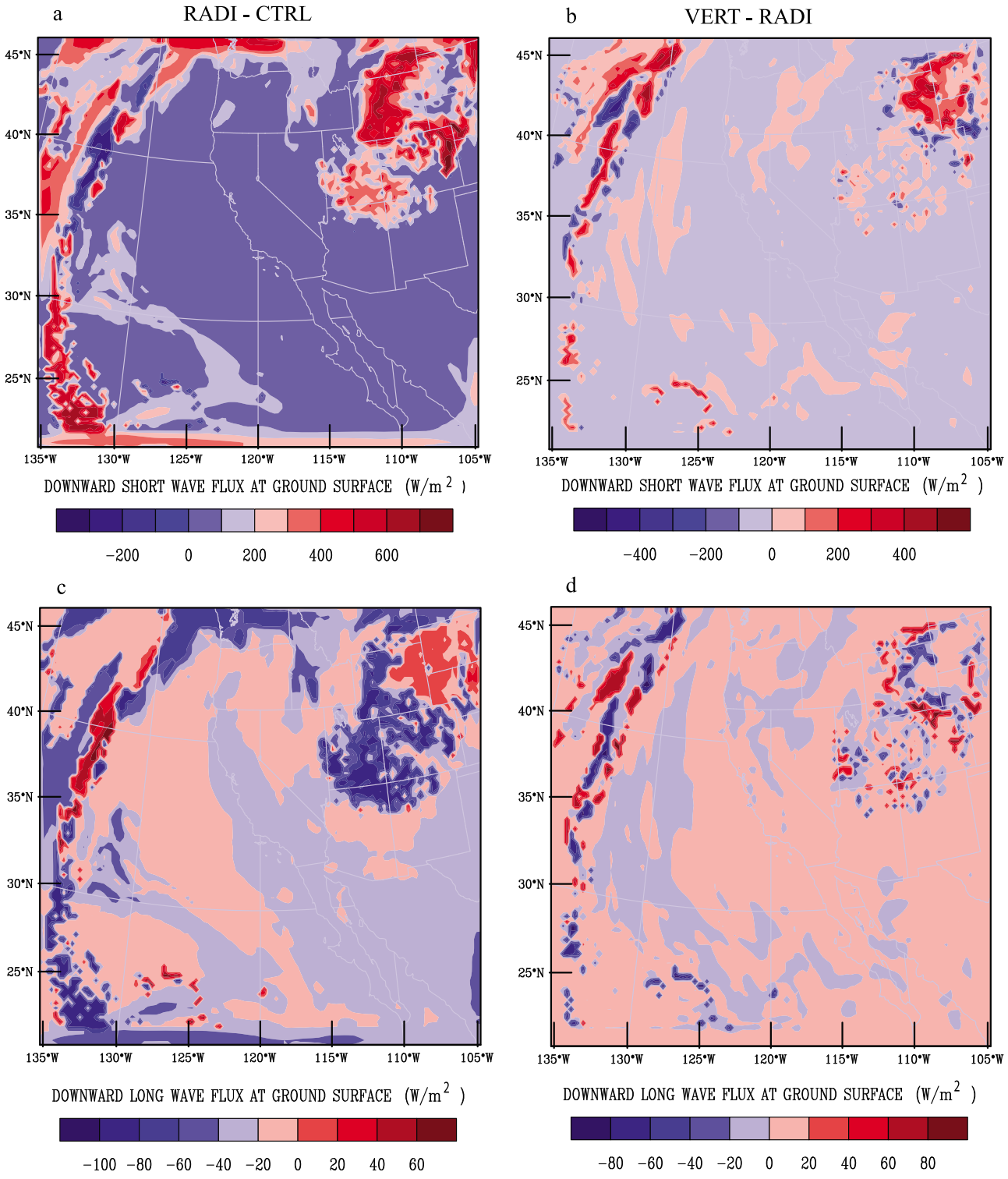

Figure 4. Simulated differences in downward (a and b) shortwave flux and (c and d) longwave flux at surface between RADI and CTRL (Figures 4a and 4c) and between VERT and RADI (Figures 4b and 4d) at 1800 UTC, 29 March 2007.

sampling over midlatitude and tropical areas, along with parameterization of the single-scattering properties using the data compiled by *Yang et al.* [2000]. We determined IWPs using the above parameterization for pixels that were identified as ice clouds on the basis of the MODIS thermal IR cloud phase mask program. The τ and a_e values have been archived for every cloudy pixel, which can be extracted from the MODIS L-2 cloud product data set. Uncertainties in the majority of IWP and CWP are of the order of 10%, on the basis of estimates of the uncertainties of cloud optical

Table 3. Mean and Standard Deviations of the Ice Water Path for the Domains of 35°–45°N and 105°–115°W (Region 1) and 40°–45°N and 115°–125°W (Region 2) Obtained From MODIS Observations at 1825 UTC on 29 March 2007 and Model Experiments CTRL, RADI, and VERT at 1800 UTC on 29 March 2007

Observations/ Experiments	IWP for Region 1 (g m^{-2})		IWP for Region 2 (g m^{-2})	
	Mean	SD	Mean	SD
MODIS	38.02	106.00	23.2	48.4
CTRL	43.18	62.19	30.47	56.85
RADI	41.26	61.45	25.76	56.91
VERT	60.53	152.30	43.43	114.14

depth and effective particle radius of 7% and 3% from MODIS L2 cloud product files, respectively.

[23] Table 3 lists IWP mean and standard deviation values for the two selected domains obtained from MODIS observations and CTRL and RADI simulation results. The minimum IWP that can be detected by satellite is about 1 g/m^2. For consistency, the same cutoff value is used when processing the model results for comparison with the observations. In terms of the IWP mean for Region 1, result from RADI, with a value of 41.26 g m^{-2}, is closer to that derived from satellite observations (38.02 g m^{-2}), as compared to the value determined from CTRL (43.18 g m^{-2}). The improvement in simulated mean IWP is about 5% employing the new radiation scheme. The standard deviations from model simulations are smaller than satellite observations for IWP, indicating that model results represent a smoother IWP distribution. For Region 2 where semitransparent thin cirrus clouds were present, RADI also produces a much closer agreement (25.76 g m^{-2}) with MODIS observations (23.2 g m^{-2}) for IWP, with an improvement of about 20% compared to CTRL (30.47 g m^{-2}). With the inclusion of the new radiation/cloud microphysics parameterizations in WRF, the simulated IWPs appear to be more consistent with the values derived from satellite observations, especially for thin cirrus clouds. Since the only difference between experiments CTRL and RADI is the use of different radiation schemes, it reveals that radiation plays an important role in the simulation of cirrus clouds as indicated by cloud-resolving model results [*Starr and Cox*, 1985; *Gu and Liou*, 2000] and that a more physically based radiation is needed in association with the simulations of cirrus clouds.

[24] We also compare the simulated cloud fraction with MODIS observations for Region 1 and 2 as shown in Table 4. Ice cloud pixels are identified by the MODIS cloud mask program on the basis of the thermal infrared window channel brightness temperature difference threshold and the 1.38 μm reflectance tests. Because of the relatively high threshold value of the latter test, some optically thin ice cloud pixels are missed in this detection scheme [*Roskovensky and Liou*, 2003]. For this reason, the actual cirrus cloud fraction could be higher. The simulated cirrus cloud fraction is comparable to but somewhat larger than observed values. The simulation results could have been closer to the "real" values given the fact that MODIS underestimates the ice cloud fraction. For Region 1, the simulated cloud covers are larger than MODIS observations (~42%), where RADI produces the best agreement (~47%). For Region 2, comparison between the two is much closer, with differences less than 1%.

[25] We then compare the model-simulated CWP and IWP with corresponding MODIS observations for Region 1. Figure 5 shows the histograms for CWP and IWP determined from observations and simulated from CTRL and RADI experiments for this region, where the x axis represents the natural logarithm value of CWP/IWP. Because the model grid points are much fewer than the number of satellite observations, we compare the CWP/IWP frequency shape and the percentages of the CWP/IWP frequency. The CWP distribution simulated from RADI, with a maximum frequency located between ~5 and 6 shows a closer comparison with observations than that from CTRL, which has a maximum between 7 and 8. About 60% of the observed CWP illustrates ln (CWP) values between ~4 and 6, representing a sharper shape, while only about 20% of simulated CWP presents in this same range, with a much smoother shape of the CWP distribution (Figures 5a–5c). Comparison between observed CWP and IWP shows that the total number of pixels for IWP is much less than that for CWP, that both ln (CWP) and ln (IWP) peak between 5 and 6, and that the shape of the distribution of ln (IWP) is narrower than that of ln (CWP). MODIS IWP and CWP were determined for pixels that were identified as ice cloud and cloudy, respectively. For domain averages or histograms, CWP values include contributions from both IWPs and LWPs. Comparison of IWP distributions between model and observation results shows larger differences than that of CWP. The bulk of observed ln (IWP) is between 4 and 6, while the major portion of CTRL and RADI ln (IWP) is between 1 and 5 (Figures 5d–5f). The difference at the tail end of the histograms is due to the fact that the MODIS histogram was based on pixel-level retrieval results, while the model simulation results were computed from model grid-average values. For MODIS observations, it is possible that ice cloud pixels identified by the MODIS cloud phase mask program could contain water clouds below [*Davis et al.*, 2009]. Hence the computed IWP from the MODIS total cloud optical depth might have included the contributions of liquid water path (LWP), which could explain the similarity in comparison between observed CWP and IWP. Additionally, MODIS cloud mask could miss optically thin cirrus cloud pixels owing to limitation of the 1.38 μm reflectance test [*Roskovensky and Liou*, 2003], resulting in a smaller fraction of low IWP values than CTRL and RADI as shown in Figure 5d. Thus comparison between simulated and observed CWP would be more meaningful than the IWP counterpart in terms of cloud water frequency distribution.

Table 4. Cirrus Cloud Fraction for the Domains of 35°–45°N and 105°–115°W (Region 1) and 40°–45°N and 115°–125°W (Region 2) Obtained From MODIS Observations at 1825 UTC on 29 March 2007 and Model Experiments CTRL, RADI, and VERT at 1800 UTC on 29 March 2007

Observations/ Experiments	Cirrus Cloud Fraction for Region 1 (%)	Cirrus Cloud Fraction for Region 2 (%)
MODIS	42.33	17.00
CTRL	49.67	17.70
RADI	46.97	17.97
VERT	56.39	17.70

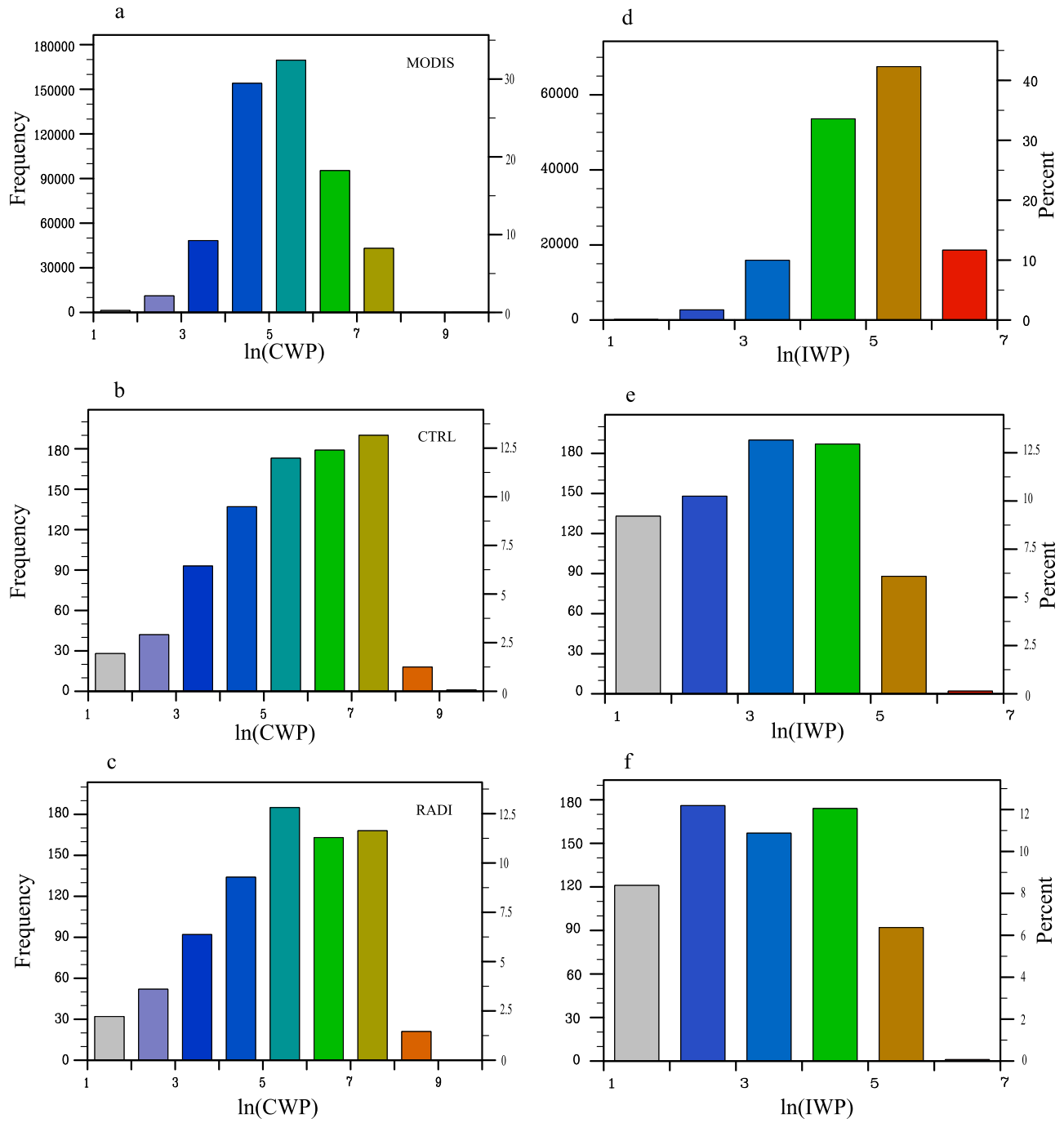

Figure 5. Histograms of (a–c) CWP and (d–f) IWP (gm^{-2}) for the domain of 35°–45°N and 105°–115°W obtained from MODIS observations at 1825 UTC on 29 March 2007 (Figures 5a and 5d), model experiment CTRL (Figures 5b and 5e), and model experiment RADI (Figures 5c and 5f) at 1800 UTC on 29 March 2007. The *x* axis represents the natural logarithm value of CWP/CWP.

[26] Vertical resolution also plays a significant role in the simulation of cirrus clouds. With an increased vertical level, the model has been shown to produce more clouds over Wyoming, Utah, and Colorado (Figure 3b). The corresponding differences in the radiative fluxes at the surface (Figures 4b and 4d), however, are not as significant as those between RADI and CTRL (Figures 4a and 4c), indicating that differences in the simulated radiation field between RADI and CTRL are not only caused by changes in the simulated cloud field but are also due to different radiation schemes. The mean IWP for the area of Wyoming, Utah, and Colorado (Region 1) at 1800 UTC on 29 March 2007 is about 60.53 g m^{-2}, with a standard deviation of about 152.3 g m^{-2}, larger than those obtained from CTRL and RADI. This is because an enhanced vertical resolution can significantly influence the vertical velocity field and the associated regional circulation discussed in the following. Simulated IWPs associated with the frontal system have also been

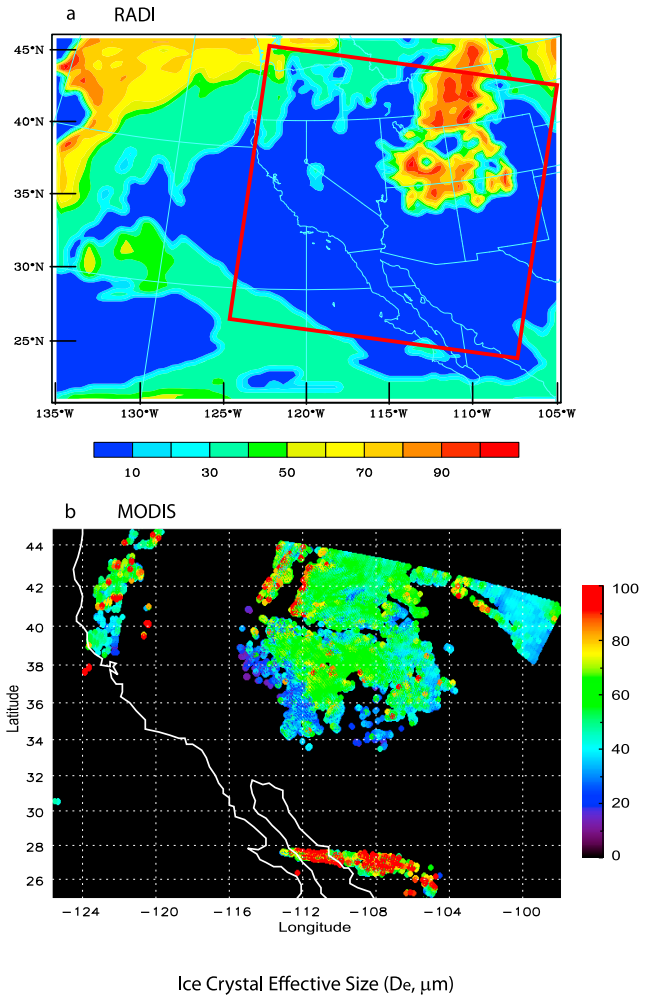

Figure 6. (a) Column-averaged ice crystal mean effective size D_e (μm) simulated from experiment RADI at 1800 UTC on 29 March 2007 and (b) MODIS-retrieved D_e (μm) for the framed region in the simulation at 1825 UTC on 29 March 2007.

enhanced with the use of a higher vertical resolution (Figure 3b). Note that the enhanced model vertical resolution does not generate results closer to observation in this case, indicating that the interactions among radiation, cloud microphysics, and dynamical processes may also be important in the model simulation of cirrus clouds. Recent work by *Fovell and Su* [2007] showed that microphysics can exert a first-order impact on hurricane track and intensity, inducing modeled landfall variations up to several hundred kilometers, demonstrated in real data and idealized simulations of hurricanes using the WRF model. Unfortunately, microphysics is one of the most poorly understood and least well validated and calibrated elements of mesoscale and cloud-resolving numerical models [e.g., *Mitchell*, 1994; *Stephens et al.*, 1990]. Identification of the mechanisms responsible for the microphysical sensitivity of cirrus simulations requires a coordinated effort using both the model results and observations and requires further in-depth studies. Although this paper does not focus on microphysics effect, we have examined another microphysics scheme, the Thompson scheme, which also predicts ice water. Using this scheme, the simulation of ice cloud cover generated by the frontal system seems to be enhanced because of improvement in the prediction of ice in outflow regions. Thin cirrus clouds over northern California, which were missing in the Lin scheme, have been generated by using the Thompson scheme. However, the ice cloud water distribution over Wyoming, Utah, and Colorado was reduced with the Thompson scheme compared to the Lin scheme.

[27] The present radiation scheme with the inclusion of cloud microphysics parameterizations can generate a mean effective ice crystal size for direct comparison with the value inferred from satellite observations. Figure 6 demonstrates this capability on the basis of a WRF simulation. We show the simulated column-averaged D_e, calculated for cloudy grid boxes only, from the RADI experiment at 1800 UTC on 29 March 2007 (Figure 6a). The distribution of D_e basically follows the cloud pattern, as shown in both observations (Figure 1e) and simulations (Figure 2e). The D_e are in the range of about 30–140 μm. Larger D_e are associated with the frontal system off the west coast of Oregon in the northwest corner of the model domain and the area covering Wyoming, Utah, and Colorado. In order to compare with satellite data, we have obtained the MODIS-retrieved D_e (Figure 6b) for the framed area in the model domain (Figure 6a). The MODIS cloud particle size has been determined from the 0.645, 1.64, 2.13, and 3.75 μm band reflectances. This parameter has been archived in an array format of 2030 by 1350 pixels with a horizontal resolution of about 1 × 1 km^2. Thus data averaging was performed so as to be comparable to the model resolution of 30 × 30 km^2. Both observations and simulations show similar patterns and comparable D_e over Wyoming, Colorado, and Utah, as well as over Oregon. The mean D_e simulated for the semi-transparent ice cloud region, 40°–45°N and 115°–125°W (Region 2), at 1800 UTC on 29 March 2007 is about 51.0 μm, in excellent agreement with the corresponding mean value of 51.4 μm obtained from MODIS observations. The production of an interactive ice crystal size is critical for the study of the effect of aerosols on ice cloud formation based on model simulations. D_e generated from VERT (not shown) are larger than RADI owing to the enhanced ice water content in this simulation.

[28] Figure 7 shows the vertical velocity together with the contour of the plane tangent velocity for CTRL (Figure 7a) and differences in the vertical velocity between RADI and CTRL (Figure 7b) and VERT and RADI (Figure 7c) along the cross section (*xz* plane; see the line in Figure 3a) near 45°N of the domain (y = 95) crossing the vortex center. Corresponding to the cyclonic circulation off the west coast, ascending motions are seen located at about 130°W (x = ~20) and extended from surface to about 10 km (Figure 7a). Stronger ascending motions are found in the same region in the experiments using the new radiation scheme (RADI-CTRL, Figure 7b), which are further strengthened with the use of higher vertical resolution (VERT-RADI, Figure 7c). These stronger vertical motions are the primary reason for the enhanced IWP in these simulations, especially in VERT. These differences are associated with changes in the radiative heating (RADI and CTRL) and the thermodynamic processes resulting from enhanced vertical model levels (VERT and RADI). The positive tangent velocities over this region indicate that the winds are coming from the south,

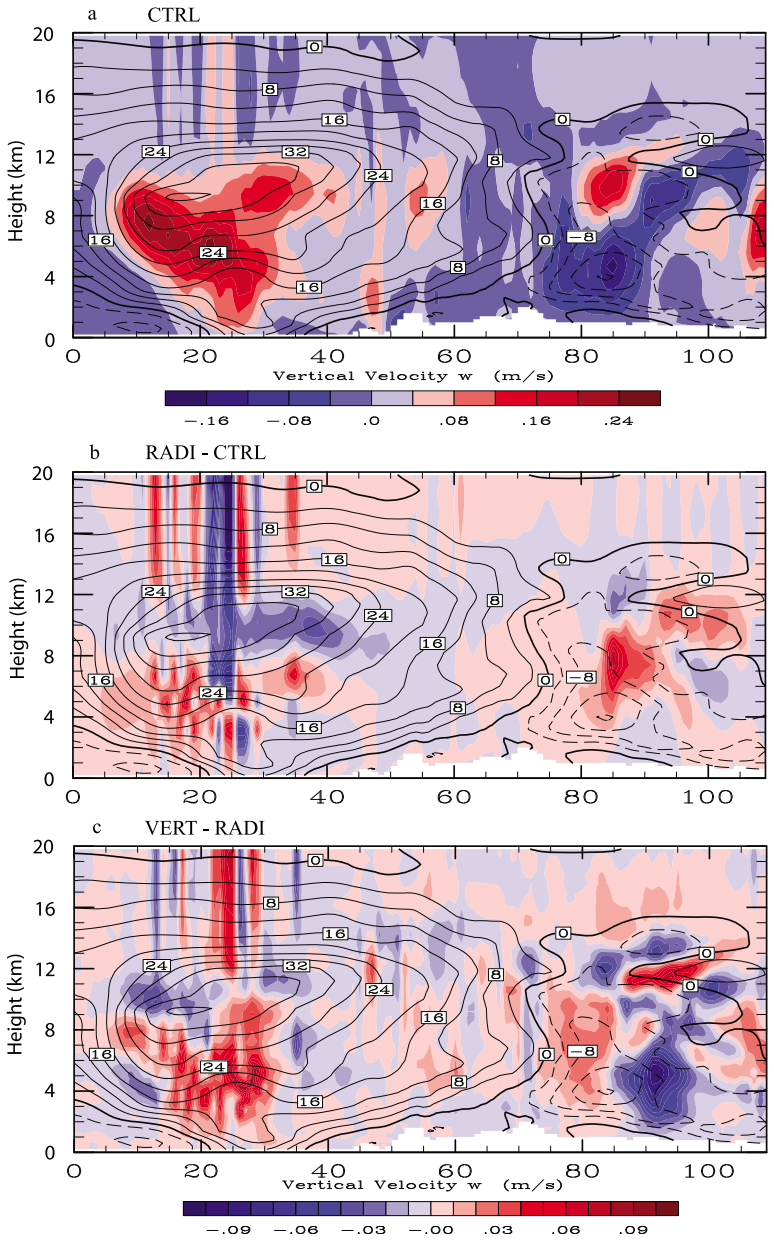

Figure 7. Vertical velocity (m/s) profile and plane tangent velocity (contour, m/s) at 1800 UTC, 29 March 2007, for (a) CTRL, (b) differences in vertical velocity between the experiments RADI and CTRL, and (c) differences in vertical velocity between the experiments VERT and RADI, at a cross section (*xz* plane) near the northern edge of the domain crossing the vortex center.

west, or southwest in front of the trough of the frontal system where clouds and precipitation are generated. The negative tangent velocity near the east side of the domain indicates that the winds are coming from the north, east, or northeast and corresponds to downward velocities in the lower troposphere in this region. However, upward motions appear above the downward velocity region near 110°W (x = 80~85) between 8 and 12 km, different from the frontal system where the ascending motions extend from surface to about 10 km, which is the primary reason for the formation of cirrus clouds in the area over Wyoming as well as a few other states to the south. Again, stronger upward air motions are found in this region in RADI and VERT, corresponding to larger IWPs in the corresponding simulations (Figure 3). Downdraft is seen to the east of upward winds associated with regional circulation and is connected to the downward motion below the uplift. In experiments RADI and VERT, we observe that the regional uplift and downdraft have both been strengthened.

4. Conclusions

[29] The numerical simulation of high cirrus clouds is a complex and difficult scientific task in regional weather and

climate modeling studies. The capability of WRF in the simulation of cirrus clouds has been examined and validated using satellite observations, with a focus on the effects of radiative processes and vertical model resolution. We incorporate in WRF a new radiation module, referred to as the Fu-Liou-Gu scheme, which is an improvement particularly in reference to parameterization of the single-scattering properties of ice crystal size and shape. A number of real-time WRF simulations have been carried out for cirrus cases that were observed in the coastal and western United States on 29–30 March 2007 and compared with available observations from MODIS and GOES-IR images over the same areas. We have demonstrated that WRF can reproduce reasonably well the observed cirrus cloud fields and their movement and dissipation processes, especially those associated with the large-scale frontal system.

[30] Radiative processes are important in cirrus cloud simulations by affecting the vertical thermal structure and hence convection. With the newly implemented radiation scheme, the simulations of cloud cover and IWP have been improved for cirrus clouds, with a more consistent comparison with the corresponding MODIS observations in terms of the CWP and IWP means and the CWP frequency distribution, especially for optically thin cirrus with an improvement of about 20% in simulated mean IWP. Additionally, we presented model-simulated ice crystal mean effective sizes and showed the results are in line with the data derived from MODIS observations. We have also illustrated that adding vertical layers in the original WRF above about 500 mbar substantially enhances simulated cloud water owing to its impact on vertical velocity field and the associated regional circulation. Note that a more physically based radiation scheme does not necessarily generate better model results owing to the intricate coupling among all the components in the model. Further studies are needed in association with the combine effects of radiation and cloud microphysics processes.

[31] Finally, we wish to point out that the newly implemented radiation module, the Fu-Liou-Gu scheme, has been demonstrated to work well in the WRF model and can be used for studies related to cirrus cloud formation and evolution and aerosol-cloud-radiation interactions, via the production of ice crystal size in addition to IWP.

[32] **Acknowledgments.** This research has been supported by AFOSR grant FA9550-07-1-0408, NASA grant NNX08AN69G, NSF grant ATM-0924876, and JPL/NASA SURP program.

References

Baum, B., et al. (2000), Remote sensing of cloud properties using MODIS Airborne Simulator imagery during SUCCESS: 2. Cloud thermodynamic phase, *J. Geophys. Res.*, *105*, 11,781–11,792, doi:10.1029/1999JD901090.

d'Almeida, G. A., P. Koepke, and E. P. Shettle (1991), *Atmospheric Aerosols: Global Climatology and Radiative Characteristics*, 561 pp., A. Deepak, Hampton, Va.

Davis, S. M., L. M. Avallone, B. H. Kahn, K. G. Meyer, and D. Baumgardner (2009), Comparison of airborne in situ measurements and Moderate Resolution Imaging Spectroradiometer (MODIS) retrievals of cirrus cloud optical and microphysical properties during the Midlatitude Cirrus Experiment (MidCiX), *J. Geophys. Res.*, *114*, D02203, doi:10.1029/2008JD010284.

DeMott, P. J., M. P. Meyers, and W. R. Cotton (1994), Parameterization and impact of ice initiation processes relevant to numerical model simulations of cirrus clouds, *J. Atmos. Sci.*, *51*, 77–90, doi:10.1175/1520-0469(1994)051<0077:PAIOII>2.0.CO;2.

Dudhia, J. (1989), Numerical study of convection observed during the winter monsoon experiment using a mesoscale two-dimensional model, *J. Atmos. Sci.*, *46*, 3077–3107, doi:10.1175/1520-0469(1989)046<3077:NSOCOD>2.0.CO;2.

Fels, S. B., and M. D. Schwarzkopf (1975), The simplified exchange approximation: A new method for radiative transfer calculations, *J. Atmos. Sci.*, *32*, 1475–1488, doi:10.1175/1520-0469(1975)032<1475:TSEAAN>2.0.CO;2.

Forster, P. V., et al. (2007), Changes in atmospheric constituents and in radiative forcing, in *Climate Change 2007: The Physical Science Basis. Contribution of Working Group I to the Fourth Assessment Report of the Intergovernmental Panel on Climate Change*, edited by S. Solomon et al., pp. 129–234, Cambridge Univ. Press, New York.

Fovell, R. G., and H. Su (2007), Impact of cloud microphysics on hurricane track forecasts, *Geophys. Res. Lett.*, *34*, L24810, doi:10.1029/2007GL031723.

Fu, Q., and K. N. Liou (1992), On the correlated *k*-distribution method for radiative transfer in nonhomogeneous atmospheres, *J. Atmos. Sci.*, *49*, 2139–2156, doi:10.1175/1520-0469(1992)049<2139:OTCDMF>2.0.CO;2.

Fu, Q., and K. N. Liou (1993), Parameterization of the radiative properties of cirrus clouds, *J. Atmos. Sci.*, *50*, 2008–2025, doi:10.1175/1520-0469(1993)050<2008:POTRPO>2.0.CO;2.

Fu, Q., K. N. Liou, M. C. Cribb, T. P. Charlock, and A. Grossman (1997), Multiple scattering parameterization in thermal infrared radiative transfer, *J. Atmos. Sci.*, *54*, 2799–2812, doi:10.1175/1520-0469(1997)054<2799:MSPITI>2.0.CO;2.

Gu, Y., and K. N. Liou (2000), Interaction of radiation, microphysics, and turbulence in the evolution of cirrus clouds, *J. Atmos. Sci.*, *57*, 2463–2479, doi:10.1175/1520-0469(2000)057<2463:IORMAT>2.0.CO;2.

Gu, Y., J. Farrara, K. N. Liou, and C. R. Mechoso (2003), Parameterization of cloud-radiation processes in the UCLA general circulation model, *J. Clim.*, *16*, 3357–3370, doi:10.1175/1520-0442(2003)016<3357:POCPIT>2.0.CO;2.

Gu, Y., K. N. Liou, Y. Xue, C. R. Mechoso, W. Li, and Y. Luo (2006), Climatic effects of different aerosol types in China simulated by the UCLA general circulation model, *J. Geophys. Res.*, *111*, D15201, doi:10.1029/2005JD006312.

Gu, Y., K. N. Liou, W. Chen, and H. Liao (2010), Direct climate effect of black carbon in China and its impact on dust storms, *J. Geophys. Res.*, *115*, D00K14, doi:10.1029/2009JD013427.

Gultepe, I., and D. O'C. Starr (1995), Dynamical structure and turbulence in cirrus clouds: Aircraft observations during FIRE, *J. Atmos. Sci.*, *52*, 4159–4182, doi:10.1175/1520-0469(1995)052<4159:DSATIC>2.0.CO;2.

Hess, M., P. Koepke, and I. Schult (1998), Optical properties of aerosols and clouds: The software package OPAC, *Bull. Am. Meteorol. Soc.*, *79*, 831–844, doi:10.1175/1520-0477(1998)079<0831:OPOAAC>2.0.CO;2.

Heymsfield, A. J., and R. M. Sabin (1989), Cirrus crystal nucleation by homogeneous freezing of solution droplets, *J. Atmos. Sci.*, *46*, 2252–2264, doi:10.1175/1520-0469(1989)046<2252:CCNBHF>2.0.CO;2.

Heymsfield, A. J., et al. (2006), Effective radius of ice particle populations derived from aircraft probes, *J. Atmos. Oceanic Technol.*, *23*, 361–380, doi:10.1175/JTECH1857.1.

Inness, P. M., J. M. Slingo, S. J. Woolnough, R. B. Neale, and V. D. Pop (2001), Organization of tropical convection in a GCM with varying vertical resolution: Implications for the simulation of the Madden-Julian oscillation, *Clim. Dyn.*, *17*, 777–793, doi:10.1007/s003820000148.

Jensen, E. J., O. B. Toon, D. L. Westphal, S. Kinne, and A. J. Heymsfield (1994a), Microphysical modeling of cirrus: 1. Comparison with 1986 FIRE IFO measurements, *J. Geophys. Res.*, *99*(D5), 10,421–10,442, doi:10.1029/93JD02334.

Jensen, E. J., O. B. Toon, D. L. Westphal, S. Kinne, and A. J. Heymsfield (1994b), Microphysical modeling of cirrus: 2. Sensitivity studies, *J. Geophys. Res.*, *99*(D5), 10,443–10,454, doi:10.1029/94JD00226.

Lacis, A. A., and J. E. Hansen (1974), A parameterization for the absorption of solar radiation in the Earth's atmosphere, *J. Atmos. Sci.*, *31*, 118–133, doi:10.1175/1520-0469(1974)031<0118:APFTAO>2.0.CO;2.

Li, G., Y. Wang, and R. Zhang (2008), Implementation of a two-moment bulk microphysics scheme to the WRF model to investigate aerosol-cloud interaction, *J. Geophys. Res.*, *113*, D15211, doi:10.1029/2007JD009361.

Li, J.-L., et al. (2005), Comparisons of EOS MLS cloud ice measurements with ECMWF analyses and GCM simulations: Initial results, *Geophys. Res. Lett.*, *32*, L18710, doi:10.1029/2005GL023788.

Liou, K. N. (1986), Influence of cirrus clouds on weather and climate processes: A global perspective, *Mon. Weather Rev.*, *114*, 1167–1198, doi:10.1175/1520-0493(1986)114<1167:IOCCOW>2.0.CO;2.

Liou, K. N. (1992), *Radiation and Cloud Processes in the Atmosphere*, 487 pp., Oxford Univ. Press, Oxford, U. K.

Liou, K. N., Q. Fu, and T. P. Ackerman (1988), A simple formulation of the delta-four-stream approximation for radiative transfer parameterizations, *J. Atmos. Sci.*, *45*, 1940–1948, doi:10.1175/1520-0469(1988)045<1940:ASFOTD>2.0.CO;2.

Liou, K. N., Y. Gu, Y. Que, and G. MacFarquhar (2008), On the correlation between ice water content and ice crystal size and its application to radiative transfer and general circulation models, *Geophys. Res. Lett.*, *35*, L13805, doi:10.1029/2008GL033918.

Minnis, P., J. K. Ayers, R. Palikonda, and D. Phan (2004), Contrails, cirrus trends, and climate, *J. Clim.*, *17*, 1671–1685, doi:10.1175/1520-0442(2004)017<1671:CCTAC>2.0.CO;2.

Mitchell, D. L. (1994), A model predicting the evolution of ice particle size spectra and radiative properties of cirrus clouds. Part I: Microphysics, *J. Atmos. Sci.*, *51*, 797–816, doi:10.1175/1520-0469(1994)051<0797:AMPTEO>2.0.CO;2.

Mlawer, E. J., S. J. Taubman, P. D. Brown, M. J. Iacono, and S. A. Clough (1997), Radiative transfer for inhomogeneous atmosphere: RRTM, a validated correlated-k model for the longwave, *J. Geophys. Res.*, *102*(D14), 16,663–16,682, doi:10.1029/97JD00237.

Pope, V. D., J. A. Pamment, D. R. Jackson, and A. Slingo (2001), The representation of water vapor and its dependence on vertical resolution in the Hadley Centre Climate Model, *J. Clim.*, *14*, 3065–3085, doi:10.1175/1520-0442(2001)014<3065:TROWVA>2.0.CO;2.

Roskovensky, J. K., and K. N. Liou (2003), Detection of thin cirrus using a combination of 1.38-μm reflectance and window brightness temperature difference, *J. Geophys. Res.*, *108*(D18), 4570, doi:10.1029/2002JD003346.

Ruti, P. M., D. Di Rocco, and S. Gualdi (2006), Impact of increased vertical resolution on simulation of tropical climate, *Theor. Appl. Climatol.*, *85*, 61–80, doi:10.1007/s00704-005-0174-8.

Sassen, K., and G. C. Dodd (1989), Haze particles nucleation simulations in cirrus clouds, and applications for numerical modeling and lidar studies, *J. Atmos. Sci.*, *46*, 3005–3014, doi:10.1175/1520-0469(1989)046<3005:HPNSIC>2.0.CO;2.

Schwarzkopf, M. D., and S. B. Fels (1991), The simplified exchange method revisited: An accurate, rapid method for computation of infrared cooling rates and fluxes, *J. Geophys. Res.*, *96*, 9075–9096, doi:10.1029/89JD01598.

Skamarock, W. C., J. B. Klemp, J. Dudhia, D. O. Gill, D. M. Barker, W. Wang, and J. G. Powers (2005), A description of the Advanced Research WRF Version 2, NCAR Tech. Note 468+STR, 88 pp., Natl. Cent. for Atmos. Res., Boulder, Colo.

Spencer, H., and J. M. Slingo (2003), The simulation of peak and delayed ENSO teleconnections, *J. Clim.*, *16*, 1757–1774, doi:10.1175/1520-0442(2003)016<1757:TSOPAD>2.0.CO;2.

Starr, D. O'C., and S. K. Cox (1985), Cirrus clouds. Part I: A cirrus cloud model, *J. Atmos. Sci.*, *42*, 2663–2681, doi:10.1175/1520-0469(1985)042<2663:CCPIAC>2.0.CO;2.

Starr, D. O'C., and D. P. Wylie (1990), The 27–28 October 1986 FIRE Cirrus case study: Meteorology and clouds, *Mon. Weather Rev.*, *118*, 2259–2287, doi:10.1175/1520-0493(1990)118<2259:TOFCCS>2.0.CO;2.

Stephens, G. L. (1978), Radiation profiles in extended water clouds. II: Parameterization schemes, *J. Atmos. Sci.*, *35*, 2123–2132, doi:10.1175/1520-0469(1978)035<2123:RPIEWC>2.0.CO;2.

Stephens, G. L., S. Tsay, P. W. Stackhouse Jr., and P. J. Flatau (1990), The relevance of the microphysical and radiative properties of cirrus clouds to climate and climate feedback, *J. Atmos. Sci.*, *47*, 1742–1754, doi:10.1175/1520-0469(1990)047<1742:TROTMA>2.0.CO;2.

Tegen, I., and A. A. Lacis (1996), Modeling of particle size distribution and its influence on the radiative properties of mineral dust aerosol, *J. Geophys. Res.*, *101*(D14), 19,237–19,244, doi:10.1029/95JD03610.

Tompkins, A. M., and K. A. Emanuel (2000), The vertical resolution sensitivity of simulated equilibrium tropical temperature and water vapor profiles, *Q. J. R. Meteorol. Soc.*, *126*, 1219–1238, doi:10.1256/smsqj.56501.

Wallace, J. M., and P. V. Hobbs (1977), *Atmospheric Science: An Introductory Survey*, 467 pp., Academic, San Diego, Calif.

Yang, P., K. N. Liou, K. Wyser, and D. Mitchell (2000), Parameterization of the scattering and absorption properties of individual ice crystals, *J. Geophys. Res.*, *105*(D4), 4699–4718, doi:10.1029/1999JD900755.

Yang, P., et al. (2005), Scattering and absorption property database for nonspherical ice particles in the near- through far-infrared spectral region, *Appl. Opt.*, *44*, 5512–5523, doi:10.1364/AO.44.005512.

Zhang, F., Q. Zeng, Y. Gu, and K. N. Liou (2005), Parameterization of the absorption of H_2O continuum, CO_2, O_2, and other trace gases in the Fu-Liou solar radiation program, *Adv. Atmos. Sci.*, *22*, 545–558, doi:10.1007/BF02918487.

Zhang, Y., Y. Pan, K. Wang, J. D. Fast, and G. A. Grell (2010), WRF/Chem-MADRID: Incorporation of an aerosol module into WRF/Chem and its initial application to the TexAQS2000 episode, *J. Geophys. Res.*, *115*, D18202, doi:10.1029/2009JD013443.

R. Fovell, Y. Gu, K. N. Liou, and S. C. Ou, Joint Institute for Regional Earth System Science and Engineering, Department of Atmospheric and Oceanic Sciences, University of California, Los Angeles, CA 90095, USA. (gu@atmos.ucla.edu)